A numerical model for the evolution of internal structure of cavitation cloud

Tezhuan Du, Yiwei Wang, Lijuan Liao, and Chenguang Huang

Citation: Physics of Fluids **28**, 077103 (2016); doi: 10.1063/1.4958885
View online: http://dx.doi.org/10.1063/1.4958885
View Table of Contents: http://scitation.aip.org/content/aip/journal/pof2/28/7?ver=pdfcov
Published by the AIP Publishing

PHYSICS OF FLUIDS **28**, 077103 (2016)

A numerical model for the evolution of internal structure of cavitation cloud

Tezhuan Du, Yiwei Wang, Lijuan Liao, and Chenguang Huang[a)]
Institute of Mechanics, Chinese Academy of Sciences, Beijing 100190, China

(Received 24 June 2015; accepted 3 July 2016; published online 21 July 2016)

Bubble size distributions in cloud cavitation are important in cavitating flows. In this study, a numerical model was developed to study the evolution of the internal structure of cloud cavitation. The model includes (1) an evolution equation of bubble number density, which considers the bubble breakup effect and (2) the multiphase Reynolds-averaged Navier–Stokes equations with a modified cavitation model for background cavitating flows. The proposed model was validated with a flow over a projectile. Results show that the numerical model can predict the evolution of the internal structure of cloud cavitation. Comparisons of the proposed model and Singhal model were discussed. The effects of re-entrant jet and bubble number density on cavitating flows were also investigated. *Published by AIP Publishing.* [http://dx.doi.org/10.1063/1.4958885]

I. INTRODUCTION

Cavitation is a key issue in high-speed underwater propulsion and can result in structure failure[1] and acoustic emissions.[2] Cavitating flow can exhibit a number of different types of cavitation, which are classified according to the shape of the interfaces into the following regimes: traveling bubble cavitation, vortex cavitation, and attach cavitation. Microbubbles in liquid moving with the flow are typical cavitation nuclei. These bubbles expand and become macroscopic cavitation bubbles as they pass through regions where pressure drops below the vapor pressure.[3,4] These cavitation bubbles are carried by the flow and then collapse in the region of pressure recovery downstream.[5] Vortex cavitation is another typical cavitation pattern; in this type, cavitation preferably develops in the vortex core, where pressure is sufficiently low because of centrifugal forces.[6] This type of cavitation is commonly observed on marine propellers or pump impellers, which produce such a vortex at the tip of each of the blades.[7] In contrast to traveling bubble cavitation, attached cavitation attaches to hydrofoils or projectiles in a quasi-permanent way. This type can be also called as sheet cavitation because it develops the shape of a sheet.[8,9] Sheet cavitation is accompanied by a highly unsteady trailing edge.[10,11] A sheet cavity may sometimes behave violently unsteady, in which case, large cavity clouds are shed periodically. Periodic formation and collapse of a cavity cloud are termed as cloud cavitation.[12]

Cloud cavitation, which consists of a large amount of small bubbles, is one of the most common types of cavitation for vessels and projectiles. Pressure pulse generated by bubble collapse in cloud cavitation is usually considered to be the major cause of structure failure and noise radiation. The internal structure of cloud cavitation must be determined to understand the generation and accurately predict collapse pressure.

In the last decades, considerable efforts have been devoted to numerical simulations of cavitating flow. Most of the researches were focused on homogeneous flow modeling, which is based on the Navier–Stokes (N-S) equations of the mixture phase.[13–17] Additional formulas are required to close the system of equations because of the introduction of variable mixture density; these formulas can be categorized into two major types: equilibrium method and phase-change method.

[a)]Author to whom correspondence should be addressed. Electronic mail: huangcg@imech.ac.cn

In the equilibrium method, the equation of the state covering all possible fluid states (i.e., liquid, vapor, and mixture) is constructed and solved with N-S equations.[13] In the phase-change method, the phase change between liquid and vapor is modeled by the transport equation of the vapor phase with phase change rate as source term. Kubota,[14] Merkle,[15] Kunz,[16] and Singhal[17] proposed several cavitation models based on the phase-change method. Örley,[18] Egerer,[19] and Gavaises[20] utilized the cavitation model and LES model to accurately predict cavitating flows. These models are used to simulate cavitating flows in many applications, such as hydrofoils, projectiles, and turbo machines. However, cavitation modeling can only provide macrosolutions of vapor volume fraction; hence, the micromechanism of cavitation evolution remains unknown. The evolution of cloud cavitation includes various microphysical processes, such as bubble collapse and development of re-entrant jet; the evolution is also highly related to the distribution of bubbles in terms of size and number. For example, bubble clusters with different distributions may lead to different collapse pressures because of the interaction of bubbles under identical vapor volume fractions. Therefore, a numerical model considering the internal structure of cloud cavitation is essential to understand bubble evolution and improve the accuracy of predicting bubble collapse pressure.

Similar considerations of modeling small particle distributions can be determined in many chemical engineering simulations. A statistical model of the dispersed phase is usually adopted in dispersed flows to describe the distribution of particle size,[21] in which the evolution of the distribution function is governed by a Boltzmann-type equation. Martínez-Bazán[22,23] proposed a model for the breakup of an air bubble injected into a fully developed turbulent flow, and the validation was made by comparing the predicted results with the measurement data. Evans[24] developed a population balance model to predict bubble size distribution and void fraction in the wake region below a ventilated gas cavity in the downward pipe flow. Unlike the chemical engineering applications, in which most models were based on the steady state condition and fully developed homogeneous turbulence, the cavitating flows with the evolution of cloud cavitation are highly unsteady and more complex in terms of flow physics. For example, a re-entrant jet forms at the closure of cavitation and goes through the vapor cavity.[25] The interaction of the re-entrant jet and cavitation are sources of instability.[11,25–27] The formation of cloud cavitation is related to the re-entrant jet[12,28] and proceeds simultaneously with phase changes between liquid and vapor.[29]

In this study, the evolution model of bubble number density is proposed to simulate bubble breakup and transportation. A numerical strategy is established to solve flow with cloud cavitation by combining the developed model with modified full cavitation model. This strategy is validated through simulation of cavitating flow around a projectile. The solutions can predict the evolution of both the outline and internal structures of cloud cavitation. These solutions are compared with experimental observations.

II. EVOLUTION MODEL OF BUBBLE NUMBER DENSITY

Cavitation cloud is normally a bubble cluster, which consists of numerous small bubbles with various sizes. Bubble–bubble interaction plays an essential role in the collapse of bubble cluster and strengthens while the bubble cluster becomes increasingly compact. Given a homogeneous bubble cluster, the vapor volume fraction α can be related to the bubble number density n and the averaged bubble size $\bar{r}$ as

$$\alpha = \frac{4}{3} n \pi \bar{r}^3. \tag{1}$$

The original homogeneous cavitation models can provide vapor volume fraction only. However, information about the internal structure of cloud cavitation, such as bubble number density and average bubble size, remains unknown. In this work, we introduce a new transport equation of bubble number density to the cavitation model to solve the internal structure of cavitation. The transport equation of bubble number density can be constructed as follows:

$$\frac{\partial}{\partial t}(\rho_m n) + \nabla \cdot (\rho_m \vec{u} n - \Gamma_m \nabla n) = S_n, \tag{2}$$

where

$\rho_m = \alpha_v\rho_v + (1-\alpha_v)\rho_l$ denotes the density of the mixture phase,

α_v is the volume fraction of the vapor phase,

Γ_m is the diffusion coefficient,

S_n is the source term involving bubble breakup and coalescence. In the present work, only the effect of bubble breakup is considered.

We obtain the following simplified transport equation by neglecting the diffusion effect of bubbles:

$$\frac{\partial}{\partial t}(\rho_m n) + \nabla\cdot(\rho_m \vec{u} n) = S_n. \tag{3}$$

Assuming the vapor volume fraction being constant during bubble breakup, then α can be considered a constant when bubbles break up. We obtain the following by taking the derivative of both sides of Eq. (1):

$$\frac{\partial n}{\partial t} = -\frac{3\alpha}{4\pi\bar{r}^6}\frac{\partial \bar{r}^3}{\partial t}, \tag{4}$$

where $\frac{\partial \bar{r}}{\partial t}$ represents the variation in the average bubble radius caused by bubble breakup and $\frac{\partial n}{\partial t}$ represents the variation in bubble number density caused by bubble breakup. Thus, the source term of Eq. (3) can be written as follows:

$$S_n = \rho_m\frac{\partial n}{\partial t} = -\frac{3\rho_m\alpha}{4\pi\bar{r}^6}\frac{\partial \bar{r}^3}{\partial t}. \tag{5}$$

The average bubble size is presented by the following:

$$\bar{r}^3 = \int_0^\infty f(t,r)r^3 dr, \tag{6}$$

where $f(t,r)$ is the probability density function of bubble size at time t.

The cyclic behavior of cloud cavitation is related to the development of the re-entrant jet, and turbulent fluctuations of the re-entrant jet presumably result in the breakup of cavitation bubbles. The bubble breakup model in turbulent flows is derived to construct the source term in Subsection II A.

A. Bubble breakup model

Bubbles break up in turbulent flows when the velocity of turbulent fluctuations exceeds the threshold value. Hence, bubbles break up in turbulent flows when the bubble size exceeds a critical value, which is related to turbulent fluctuations and surface tension. According to Sosinovich,[30] the evolution equation of the probability density function of bubble size can be written as

$$\frac{\partial f(t,r)}{\partial t} = -\int_0^r \frac{f(t,r)}{\tau(r)}\omega(r_1,r)dr_1 + \int_r^\infty \frac{f(t,R)}{\tau(R)}\omega(r,R)dR, \tag{7}$$

where $\tau(r)$ represents the breakup time of a bubble of radius r, and the breakup function $\omega(r,R)$ represents the probability of a bubble of size R breaking into bubbles of size r. By neglecting the convection effect, the effects of bubble breakup on the time rate of probability density function can be divided into two parts: the first term on the right hand side of Eq. (7) represents the decrease in probability function caused by the bubbles of size r breaking into small bubbles, whereas the second term indicates the increase in probability function caused by the bubbles of radii $r_1 > r$ breaking into the bubbles of size r.

A bubble breaks into two bubbles near the critical Weber number;[31] hence, the breakup function can be presented as follows:

$$\omega(r,R) = \theta(R-r)\theta(R-a_{cr})\delta(r-\frac{R}{\sqrt[3]{2}}), \tag{8}$$

where $\theta(x)$ is the step function, and a_{cr} is the critical size and determined by the following equation:[32]

$$a_{cr}\int_0^{2a_{cr}} P(t,r)dr = (1/C_f)^{1/3}(\sigma/\rho_l)(\rho_l/\rho_a)^{1/3}, \tag{9}$$

where $C_f = 0.5$ is the drag coefficient of a spherical bubble; $\sigma = 0.0717$ N/m is the surface tension,[17] ρ_l and ρ_a denote the density of liquid and gas, respectively; $P(t,r)$ is the turbulent kinetic energy distribution over length scales and can be expressed as follows:

$$P(t,r) = \frac{k}{\sqrt{2\pi}\sigma_p}\exp\left[\frac{-1}{2\sigma_p^2}(r-L)^2\right], \tag{10}$$

where $L = C_\mu\frac{k^{3/2}}{\varepsilon}$ is the turbulence length scale, which describes the size of large energy-containing eddies in turbulent flows. k is the turbulent kinetic energy, and ε is the turbulent dissipation rate. $C_\mu = 0.1$ is a constant, and $\sigma_p = 0.005$ is the standard deviation of the distribution with its variance σ_p^2.

The bubble breakup time τ is the key parameter in the bubble breakup model, which determines the speed of bubble breakup. r and $\sqrt{k}$ can be selected as the characteristic length and velocity, respectively, because the breakup of bubbles is caused by turbulent fluctuations. Assuming that a bubble breaks up along the midsection into two bubbles, the breakup time can be written as

$$\tau(r) = a_t\frac{r}{\sqrt{k}}. \tag{11}$$

Given that surface tension impedes bubble breakup, an additional term $a_t b_t\frac{1}{\sqrt{k}r}$ is introduced into the model to determine the effect of surface tension and avoid divergence near $r = 0$. Thus, the breakup duration can be modeled as follows:

$$\tau(r) = a_t\frac{1}{\sqrt{k}}\left(r + b_t\frac{1}{r}\right), \tag{12}$$

where a_t and b_t are case-dependent and user-defined constants, respectively. The parameter b_t in the model determines bubble size corresponding to the minimum bubble breakup time, which is $r = \sqrt{b_t}$. The parameter a_t is a relaxation factor that determines the average value of bubble breakup time. $a_t = 5\times10^{-4}$ and $b_t = 10^{-6}$ m^2 are suitable for this model (Appendix).

By substituting Eq. (8) into Eq. (7), we obtain the following:

$$\frac{\partial f(t,r)}{\partial t} = -\frac{f(t,r)}{\tau(r)}\theta\left(r - a_{cr}(t)\right) + \frac{f(t,\sqrt[3]{2}r)}{\tau(\sqrt[3]{2}r)}\theta\left(\sqrt[3]{2}r - a_{cr}(t)\right). \tag{13}$$

Using Eqs. (6) and (13), we can derive the evolution equation of the average bubble size,

$$\frac{\partial\bar{r}^3}{\partial t} = \int_0^\infty\left[-\frac{f(t,r)}{\tau(r)}\theta\left(r - a_{cr}(t)\right) + \frac{f(t,\sqrt[3]{2}r)}{\tau(\sqrt[3]{2}r)}\theta\left(\sqrt[3]{2}r - a_{cr}(t)\right)\right]r^3dr, \tag{14}$$

where

$$\int_0^\infty\left[-\frac{f(t,r)}{\tau(r)}\theta\left(r - a_{cr}(t)\right)\right]r^3dr = -\int_{a_{cr}}^\infty\frac{f(t,r)}{\tau(r)}r^3dr, \tag{15}$$

$$\int_0^\infty\left[\frac{f(t,\sqrt[3]{2}r)}{\tau(\sqrt[3]{2}r)}\theta\left(\sqrt[3]{2}r - a_{cr}(t)\right)\right]r^3dr = \frac{1}{\sqrt[3]{4}}\int_{a_{cr}}^\infty\frac{f(t,r)}{\tau(r)}r^3dr. \tag{16}$$

Thus, Eq. (14) can be rearranged as follows:

$$\frac{\partial \bar{r}^3}{\partial t} = \left(\frac{1}{\sqrt[3]{4}} - 1\right) \int_{a_{cr}}^{\infty} \frac{f(t,r)}{\tau(r)} r^3 dr. \tag{17}$$

By substituting Eqs. (17) and (6) into Eq. (5), we obtain the source term in the transport equation of bubble number density,

$$S_n = -\frac{3\rho_m \alpha}{4\pi} \left[\int_0^{\infty} f(t,r) r^3 dr\right]^{-2} \left(\frac{1}{\sqrt[3]{4}} - 1\right) \int_{a_{cr}}^{\infty} \frac{f(t,r)}{\tau(r)} r^3 dr. \tag{18}$$

During the simulation, the probability density function of bubble size is presented by the following:

$$f(t,r) = \frac{1}{\sqrt{2\pi}\sigma_f} \exp\left[\frac{-1}{2\sigma_f^2}\left(r - \sqrt[3]{\alpha / \frac{4}{3}\pi n}\right)^2\right], \tag{19}$$

where σ_f is the standard deviation and set as $\sigma_f = 0.3\bar{r}$. The Gaussian size distribution agrees with the experimental results for small bubbles. However, the numerical result is smaller than the experimental measurement for large bubbles, which can be explained by the neglect of coalescence.[30]

The evolution of bubble number density can be simulated by solving Eqs. (2) and (18).

III. MODIFIED FULL CAVITATION MODEL

A cavitation model is constructed based on the full cavitation proposed by Singhal[17] to determine the influence of bubble number density on cavitating flow. The continuous equation of vapor phase can be written as follows:

$$\frac{\partial}{\partial t}(\rho_m f_v) + \nabla \bullet (\rho_m f_v \vec{u}_m) = \nabla(\gamma \nabla f_v) + Re - Rc, \tag{20}$$

where

f_v is the mass fraction of vapor and is related to the volume fraction of vapor α_v as $\alpha_v \rho_v = \rho_m f_v$,

γ is the equivalent diffusion coefficient,

Re and Rc represent the vapor generation rate and condensation rate, respectively. The continuity equations of liquid phase and vapor phase listed as follows can be used to obtain the net phase change rate:

Liquid phase:

$$\frac{\partial}{\partial t}[\rho_l(1-\alpha_v)] + \nabla \bullet \left[\rho_l(1-\alpha_v)\vec{u}_m\right] = Rc - Re. \tag{21}$$

Vapor phase:

$$\frac{\partial}{\partial t}(\rho_v \alpha_v) + \nabla \bullet (\rho_v \alpha_v \vec{u}_m) = Re - Rc. \tag{22}$$

With Eq. (22) $\times \rho_l(1-\alpha_v)$– Eq. (21) $\times \rho_v \alpha_v$, we derive the following:

$$Re - Rc = \frac{\rho_l \rho_v}{\rho_m} \frac{d\alpha_v}{dt}. \tag{23}$$

Variation in vapor volume fraction can be derived from the Rayleigh–Plesset equation,[33]

$$\rho_l R\ddot{R} + \frac{3}{2}\rho_l \dot{R}^2 + \frac{2\gamma}{R} + 4\frac{\mu}{R}\dot{R} = p_B - p_\infty, \tag{24}$$

where p_B is the pressure inside the bubble, and p_∞ is the pressure at infinity. We obtain the following by ignoring the viscous effect, surface tension, and second-order derivative of R:[17]

$$\frac{dR}{dt} = \sqrt{\frac{2}{3\rho_l}|p_\infty - p_B|}. \tag{25}$$

By setting $\bar{r} = R$, we can rewrite Eq. (1) as

$$R = \left(\frac{3}{4}\frac{\alpha_v}{n\pi}\right)^{\frac{1}{3}}. \tag{26}$$

By substituting Eq. (26) into Eq. (25), we obtain

$$\frac{d\alpha_v}{dt} = (3\alpha_v)^{\frac{2}{3}}(4n\pi)^{\frac{1}{3}}\sqrt{\frac{2}{3\rho_l}|p_\infty - p_B|}. \tag{27}$$

By combining Eqs. (23) and (27), we obtain the expression for net phase change rate as

$$Re - Rc = 3\frac{\rho_l\rho_v}{\rho_m}\left(\frac{3\alpha_v}{4n\pi}\right)^{-\frac{1}{3}}\alpha\sqrt{\frac{2|p_\infty - p_B|}{3\rho_l}}. \tag{28}$$

In this work, we only focus on the influence of bubble number density on vapor condensation rate. By combining the vapor generation rate of full cavitation model and the effects of non-condensable gas,[17] we obtain the following expressions for phase change rates:

$$Re = C_e\rho_l\frac{\rho_l\rho_v}{\rho_m}\frac{\sqrt{k}}{\sigma}\sqrt{\frac{2(p_B - p_\infty)}{3\rho_l}}(1 - \alpha_v - \alpha_g), \quad p < p_v, \tag{29}$$

$$Rc = C_c\frac{\rho_l\rho_v}{\rho_m}\left(\frac{3\alpha_v}{4n\pi}\right)^{-\frac{1}{3}}\alpha_v\sqrt{\frac{2(p_\infty - p_B)}{3\rho_l}}, \quad p > p_v, \tag{30}$$

where α_g is the volume fraction of non-condensable gas. $p_v = (p_{sat} + \frac{1}{2}p_{turb})$ is the phase change threshold pressure, p_{sat} is the saturation pressure of vapor, and $p_{turb} = 0.39\rho k$ is the turbulent pressure fluctuation. $C_e = 0.01$ and $C_c = 3.0$ are constants for phase change rates. In this study, the mixture phase consists of liquid, vapor, and non-condensable gas. Thus, the density of the mixture phase should be modified as follows:

$$\rho_m = \alpha_v\rho_v + \alpha_g\rho_g + (1 - \alpha_v - \alpha_g)\rho_l. \tag{31}$$

IV. NUMERICAL STRATEGY

The basic approach for cavitating flows consists of unsteady Reynolds averaged N-S (RANS) equations of the mixture phase. The governing equations are listed as follows:

$$\frac{\partial\rho_m}{\partial t} + \nabla\bullet(\rho_m\vec{u}_m) = 0, \tag{32}$$

$$\frac{\partial}{\partial t}(\rho_m\vec{u}_m) + \nabla\bullet(\rho_m\vec{u}_m\vec{u}_m) = -\nabla p + \nabla\bullet[\mu_m(\nabla\vec{u}_m + \nabla\vec{u}_m^T)] + \nabla\bullet(-\rho_m\overrightarrow{\vec{u}'_m\vec{u}'_m}), \tag{33}$$

where $\mu_m = \alpha_v\mu_v + \alpha_g\mu_g + (1 - \alpha_v - \alpha_g)\mu_l$ is the equivalent viscosity of the mixture phase.

In the present work, the modified RNG $k - \varepsilon$ model[25] is used to model turbulence in cavitating flows. By combining Eqs. (2), (20), (32), and (33), we obtain the governing equations for the evolution of cloud cavitation, in which each equation is solved iteratively. The numerical procedure of cloud cavitation computation is demonstrated in Figure 1.

Unsteady RANS equations combined with the modified RNG $k - \varepsilon$ model are solved by FLUENT using SIMPLEC algorithm to provide background flow information to the continuity equation of the vapor phase and transport equation of bubble number density, which are computed in

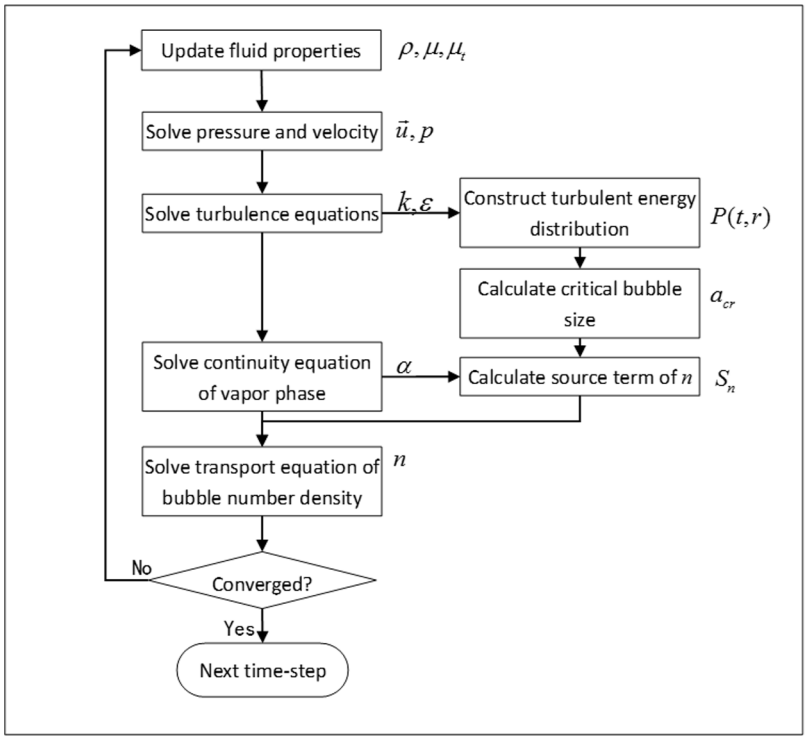

FIG. 1. Numerical procedure.

sequence. Calculation of the additional transport equation of bubble number density and its source term consumes more computing power, which depends on mesh size and resolution of the bubble size distribution function.

V. VALIDATION

Simulation of cavitating flow over a cylindrical body with 90° blunt conical head is presented in this section. The diameter of the cylinder is $D = 37.5$ mm, and the free-stream velocity is $V = 18$ m/s and the ambient pressure is 101 325 Pa. Physical properties of liquid and vapor are listed as follows:

The saturation pressure of water is set as 2367 Pa. The corresponding cavitation number and Reynolds number are $\Sigma = 0.611$ and $\mathrm{Re} = 6.75 \times 10^5$, respectively. According to experimental observations, the cavitation seems uniform in circumferential. A 2-D axisymmetric geometry is utilized in the simulation with a 350×150 structural mesh, which is depicted in Figure 2. The height of the first grid layer is 2×10^{-4} mm, which ensures that the wall y+ is of the order O(1).

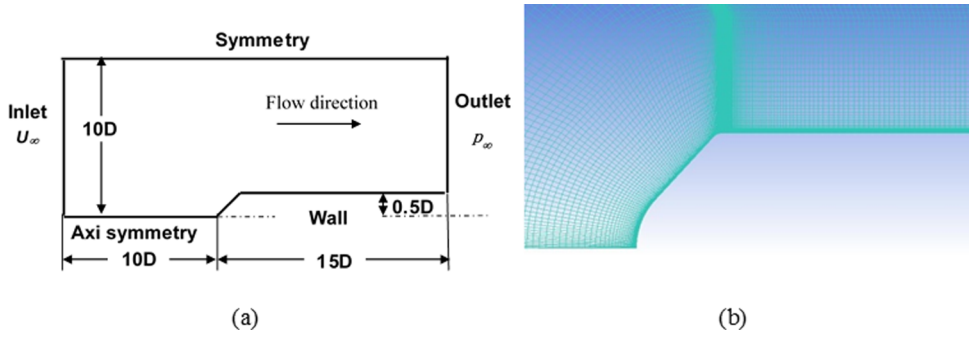

FIG. 2. CFD model setup: (a) computational domain and boundary conditions and (b) mesh.

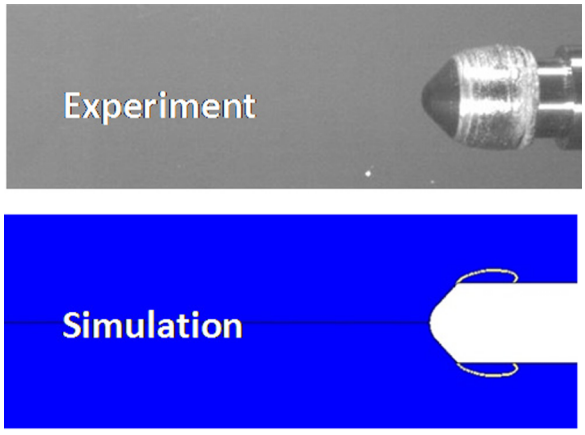

FIG. 3. Growth of sheet cavitation (t = 3 ms).

The numerical results are compared with experimental data based on Split Hopkins Pressure Bar (SHPB) launch system,[34] which can transiently accelerate the projectile and can cause slight disturbance in water tank. Prior to launching, the interior of the water tank is full of water with pressure at 1 atm. The projectile transiently obtains a velocity of 18 m/s by the SHPB launch system and is then driven by inertia. A high-speed digital camera was used to record the launch process and cavitation features with a frame grabbing speed of 5000 fps (frames per second).

Figures 3–7 illustrate the comparison of the observed cavitation (upper) and the predicted cavitation (lower). The yellow curves represent the iso-surface of vapor fraction with the value of 0.1, and the red zones in the cavitation indicate the high bubble number density area ($n \geq 10^9$), which can be regarded as cloud cavitation.

The evolution of cavitation can be divided into four stages: growth of sheet cavitation, development of re-entrant jet, detachment of cavitation cloud, and collapse of the detached cavitation cloud. When cavitation occurs, a transparent laminar void starts to grow from the shoulder of the projectile (Figure 3).

The bubbles start to break up as the re-entrant jet develops with simultaneous increase in bubble number density. The breakup process converts sheet cavitation into cloud cavitation (Figure 4).

The whole cavitation area is converted into a nontransparent cavitation cloud when the re-entrant jet reaches the shoulder of the projectile (Figure 5), where the cavitation cloud detaches and rolls downstream with mean flow until collapse (Figures 6 and 7). Meanwhile, the new attached cavitation appears at the shoulder of the projectile. The simulation results show that the formation of cloud cavitation is closely related to the re-entrant jet, which is also observed in flows over hydrofoils.[12,13]

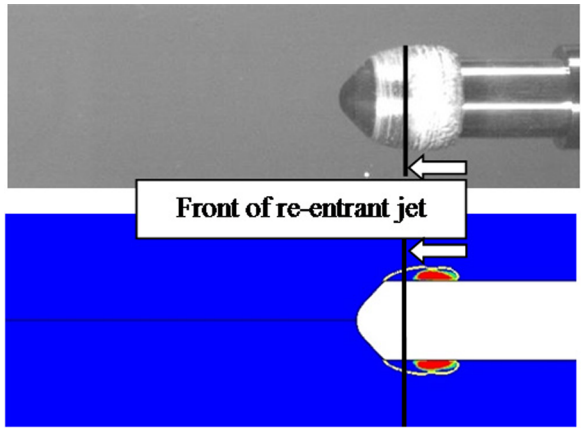

FIG. 4. Development of the re-entrant jet (t = 5 ms).

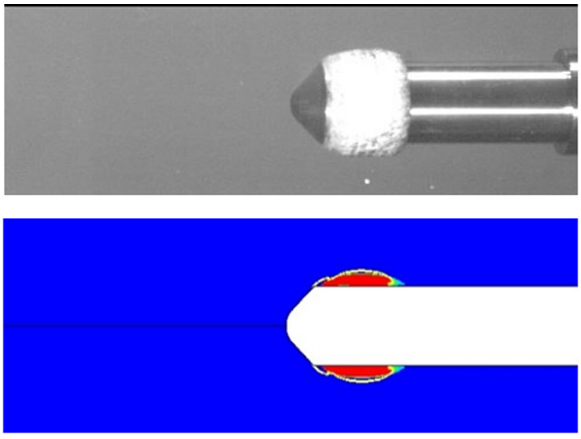

FIG. 5. Full cloud cavitation (t = 7 ms).

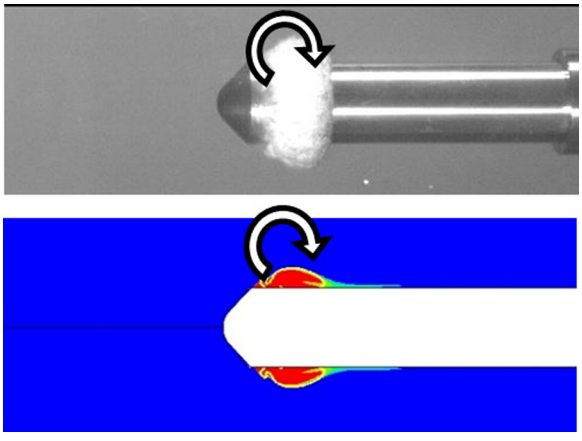

FIG. 6. Detachment of cloud cavitation (t = 9 ms).

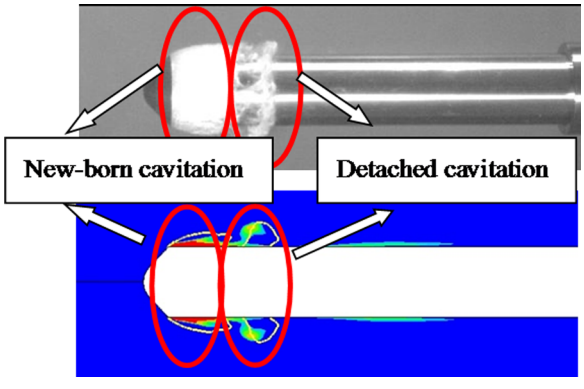

FIG. 7. Collapse of the detached cavitation (t = 13 ms).

Figure 8 illustrates the outline of cavitation and the distribution of bubble number density n. Cloud cavitation area is consistent with the region swept by the re-entrant jet. This finding confirms that the re-entrant jet breaks bubbles into small ones and forms the cavitation cloud.

Figure 9 presents the distribution of bubble number density in the cavitation region along the wall of the projectile, and the origin of X axis represents the leading edge of cavitation. Cavitation can be divided with the re-entrant jet into two parts: transparent laminar cavitation and

nontransparent cloud cavitation. Bubble number density increases rapidly at the front of the re-entrant jet and decreases close to the cavitation closure. Bubble size is not uniform in the region of cloud cavitation (Figure 10). The minimum value of $\bar{r}$ is 0.202 mm, which corresponds to the maximum n of 3.06×10^{10} m^{-3}.

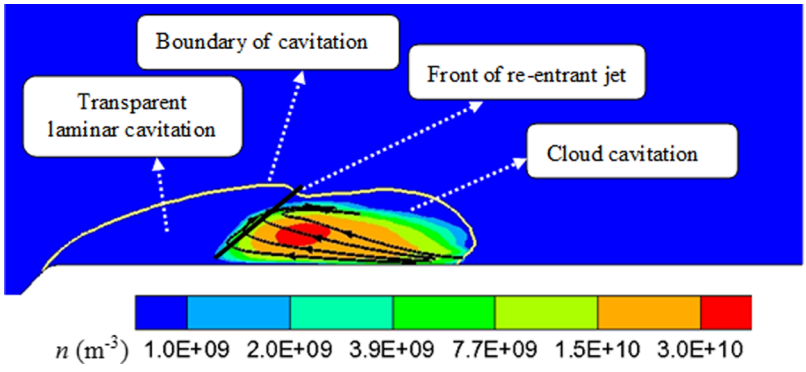

FIG. 8. Formation of cloud cavitation.

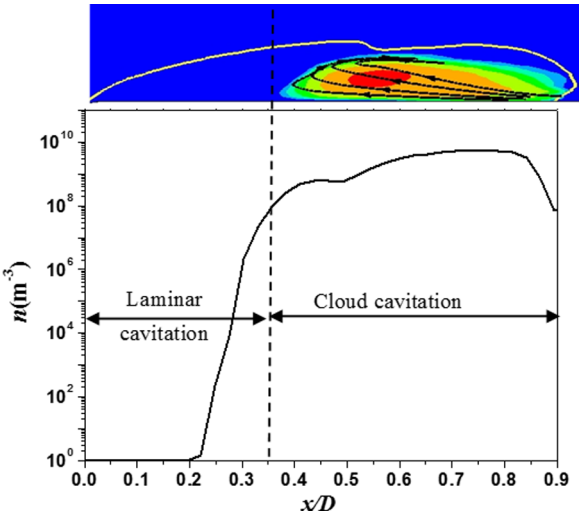

FIG. 9. Distribution of bubble number density in the cavitation (t = 5 ms).

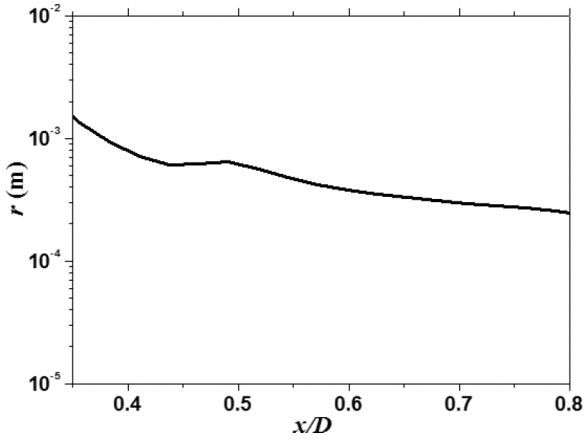

FIG. 10. Distribution of bubble size in the cavitation cloud (t = 5 ms).

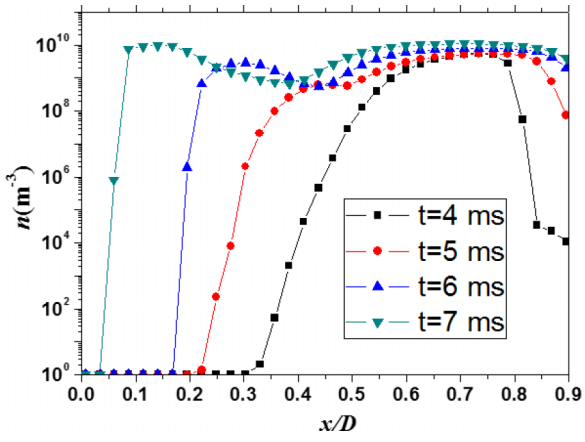

FIG. 11. Distribution of bubble number density in the cavitation.

TABLE I. Physical properties of working fluids.

Phase	Density (kg/m^3)	Viscosity (kg/m-s)
Liquid	998.2	1.00×10^{-3}
Vapor	0.5542	1.34×10^{-5}

TABLE II. Conditions of inlet velocity.

Case	Free-stream velocity (m/s)	Cavitation number	Reynolds number	Turbulent intensity (%)
1	9	0.611	6.75×10^5	1
2	12	0.611	6.75×10^5	1
3	18	0.611	6.75×10^5	1

The distribution of bubble number density along the projectile surface at different times is illustrated in Figure 11. The bubble number density inside the cavitation cloud increases as the development of re-entrant jet. And the interface of laminar cavitation and cloud cavitation will become steeper.

Comparisons of simulation results with the experimental data suggest that the proposed numerical strategy can predict the evolution of cavitation. The distribution of bubble number density solved by the proposed model can also be used to elucidate the internal structure of cloud cavitation.

VI. DISCUSSION

A. Re-entrant jet effect

To further investigate the effect of the re-entrant jet on bubble breakup, we performed additional simulations. The following conditions were utilized, considering that the velocity of the re-entrant jet is related to the inlet velocity (Tables I and II). The cavitation number and Reynolds number remain constant.

Figure 12 illustrates the predicted cavity length under different conditions of inlet velocities. Re-entrant jet meets the leading edge of the cavity at about $\frac{tV}{D} = 3.3$ and cuts the cavity off. The detached cavity rolls downstream and starts to collapse near $\frac{tV}{D} = 6.0$. Collapse of the detached cavities marked in Figure 12 represents the moment when the cavity completely collapses. The growth velocity of cavitation is proportional to the inlet velocity, and the evolution of cavities is diverse during the collapse stage.

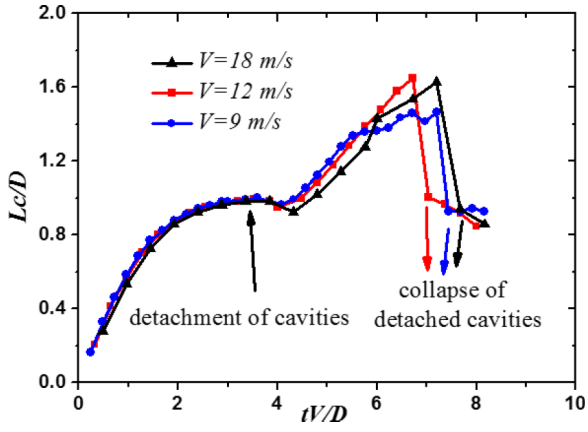

FIG. 12. Comparisons of the predicted cavity length at different velocities.

The Weber number can be given by $We = \frac{\rho_L V_{in}^2 D}{\sigma}$, where ρ_L is the liquid density, V_{in} is the inlet velocity, D is the diameter of the cylinder, σ is the surface tension. Table III shows that high velocity of the re-entrant jet results in large bubble number density and small bubble size. This observation indicates that bubble breakup intensifies with increasing re-entrant jet velocity. This finding could be due to the fact that re-entrant jet with a large velocity (or a higher Weber number) usually imports kinetic energy to the cavitation region and accelerates the process of bubble breakup.

B. Comparison with full cavitation model

The present model was compared with full cavitation model under the following conditions: V = 18 m/s, Σ = 0.611, Re = 6.75×10^5. In this case, the detached cavity cloud collapses near x/D = 1.25. Thus, a probe was set at x/D = 1.25 on the projectile surface to record pressure during the simulations. We focused on the evolution of cavitation and collapse of the detached cavity clouds. Figure 13 illustrates that cavity lengths predicted by both models are nearly the same at the growth stage. The reason is that the growth of cavities is governed by the vapor generation rate Re, and both models share the same expression of Re. The evolution of cavities differs after the detachment of cavities because of condensation rates.

The simulation results show that the present model predicts higher amplitude and frequency of collapse pressure than those derived using the Singhal model (Figure 14). The details of regions I and II in Figure 15 are illustrated. It is observed that there are three high pressure areas in region I, whereas it is much uniform in region II. These findings could be due to the fact that the present model includes the effects of bubble density.

C. Bubble–bubble interaction effect

Bubble number density plays an important role in processes in cavitating flows, including the dynamic characteristic of bubble cloud,[35] the collapse process of cavitation,[36,37] and the effective viscosity of bubbly flow.[38] The detached cavitation can be regarded as a bubble cluster. Consider

TABLE III. Re-entrant jet effect.

Case	Weber number	Velocity of the re-entrant jet (m/s)	Maximum n (10^{10}/m^3)	Minimum $\bar{r}$ (mm)
1	4.23×10^4	7.97	0.185	0.515
2	7.52×10^4	10.6	0.215	0.490
3	1.69×10^5	15.9	3.06	0.202

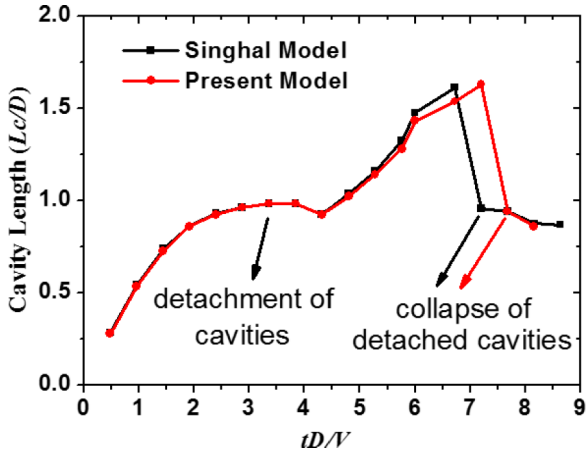

FIG. 13. Comparison of the cavity lengths predicted by the Singhal model and the present model.

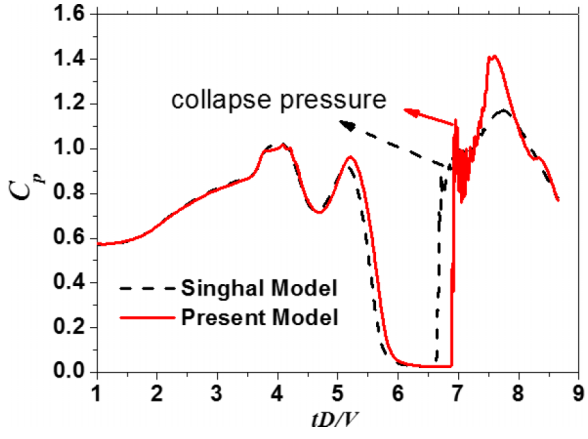

FIG. 14. Comparisons of the pressure coefficient at $x/D = 1.25$ by using the Singhal model and the present model.

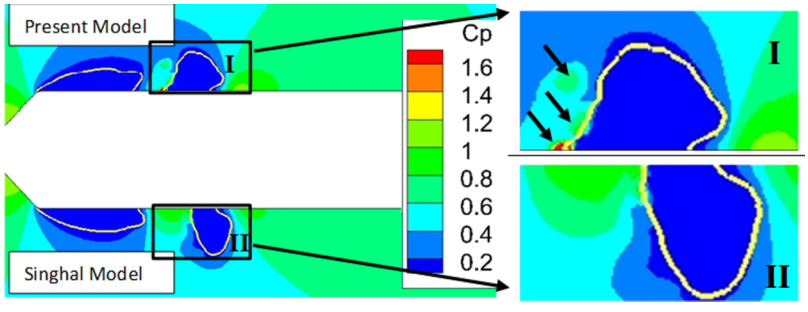

FIG. 15. Comparisons of pressure fields at $tV/D = 6.7$ by using the Singhal model and the present model.

a spherical bubble cluster consisting of uniform bubbles in an unbounded liquid (Figure 16). The volume fraction of the bubble is α, the radius of the bubble cluster is A, and the radius of the bubble is r. The strength of bubble–bubble interaction can be represented as $\beta = \alpha A^2/r^2$. High value of β corresponds to a strong interaction. While for $\beta > 1$, the interaction among bubbles cannot be ignored, and the natural frequency decreases than the frequency of the single bubble.[39,40] During collapse of the bubble cluster, an important characteristic, named geometry focusing of collapse pressure, exists. Pressure waves emitted by collapsed bubbles propagate inward, leading to the acceleration characteristic of the central bubbles and high magnitude of collapse pressure.[41]

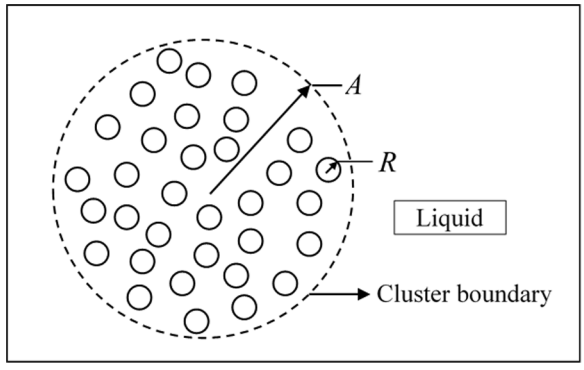

FIG. 16. Schematic of a bubble cluster.

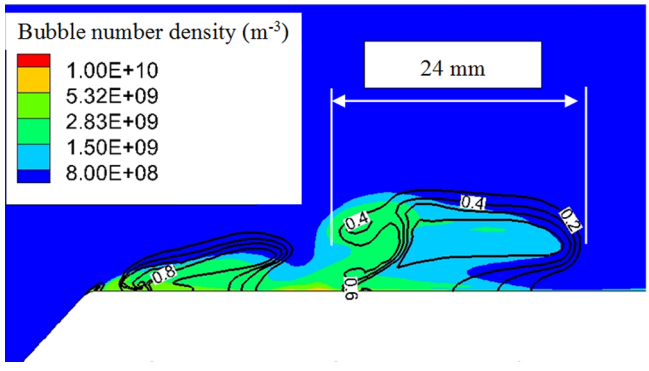

FIG. 17. Detached cavitation cloud. V = 18 m/s.

Basing on the studied cases, we can regard the detached cavitation cloud as a spherical bubble cluster (Figure 17). The vapor volume fraction can be selected as 0.2, the radius of cluster is approximately 12 mm, and the average bubble size is approximately 0.5 mm. Then, we obtain $\beta = 115$. β is considerably higher than 1, thereby indicating that the bubble–bubble interaction is intense. The distribution of bubble size is non-uniform. The same vapor volume fraction could correspond to a different bubble number density and bubble size. The cloud containing different sizes of bubbles emits a pressure wave larger than those emitted by the cloud consisting of identical bubbles.[42]

In this study, the bubble–bubble interaction is ignored. Thus, a low collapse pressure may be obtained.

VII. CONCLUSIONS

Homogeneous cavitation models can only present volume fractions of different phases, which are insufficient for cavitating flow, particularly for collapse of cloud cavitation. Different bubble sizes and bubble number densities may correspond to the same vapor fraction. The cavitation cloud of different internal structures can result in different collapse pressures because of the interaction among bubbles. The internal information of cloud cavitation is required to accurately predict collapse pressure.

In the present work, a numerical model consisting of modified full cavitation model and evolution equation of bubble number density was proposed. This model was implemented on cavitating flow over a projectile with blunt conical head and compared with experiment based on the SHPB launch system. The simulation results showed that the present model can predict a reasonable evolution of cavitation and distribution of bubble number density.

The formation of cloud cavitation is related to the re-entrant jet, and bubble breakup intensifies with increasing velocity of the re-entrant jet. Comparison of the present model with the Singhal

model was also discussed. The collapse pressure of the detached cavitation cloud is affected by bubble number density. The non-uniform distribution of bubble number density may lead to different collapse velocities. The region of cavitation cloud with high bubble number density can collapse more fiercely than the other regions. The bubble–bubble interaction in the cavitation cloud cannot be ignored and needs further study.

The proposed model can solve the distribution of bubble number density and can be used to elucidate the internal structure of cloud cavitation. The proposed numerical model can be applied to predict sheet cavitation and cloud cavitation. But how it performs in other types of cavitation (such as tip vortex cavitation and super cavitation) requires further testing. Moreover, continuous efforts should be made to improve this model. First, only bubble breakup was considered in the present model; thus, the effects of coalescence must be further studied. Second, although the breakup model was simplified, the present model remains time consuming. The proposed numerical method must be optimized to enhance computational efficiency.

ACKNOWLEDGMENTS

This research was sponsored by National Natural Science Foundation of China under Contract No. 11402276 (Tezhuan Du, Program Manager).

APPENDIX: BUBBLE BREAKUP TIME

Bubble breakup time plays an important role in the evolution of bubble number density. The parameters in the bubble breakup model should be defined for specific applications. Given that the evolution of the cloud cavitation is closely related to the re-entrant jet, the parameters of breakup time can be determined by analyzing the relationship between the development of the re-entrant jet and the process of bubble breakup. The characteristic time of the development of re-entrant jet can be defined as follows:

$$T_r = \frac{L_c}{v_r}, \tag{A1}$$

where L_c is the maximum length of the cavitation, and v_r is the velocity of the re-entrant jet.

The dimensionless time is given as the ratio of bubble breakup time to the characteristic time of the development of the re-entrant jet,

$$t' = \frac{\tau(r)}{T_r}. \tag{A2}$$

The evolution of bubble number density depends on the value of t'. The process of bubble breakup finishes as soon as the re-entrant jet sweeps over when $t' \ll 1$. By contrast, bubble number

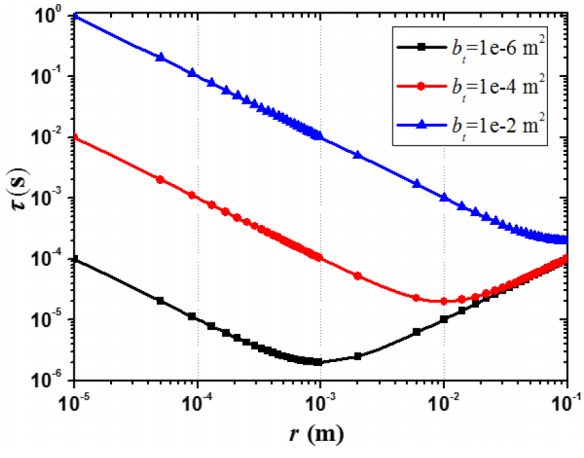

FIG. 18. Breakup time for different b_t ($a_t = 10^{-3}$, $k = 1.0$ m^2/s^2).

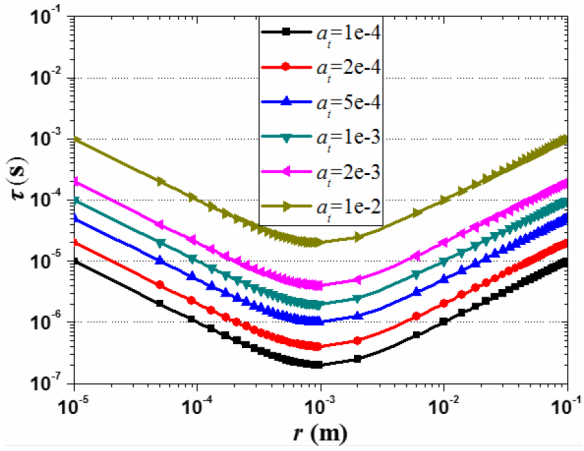

FIG. 19. Breakup time for different a_t ($b_t = 10^{-6}$ m^2, $k = 1.0$ m^2/s^2).

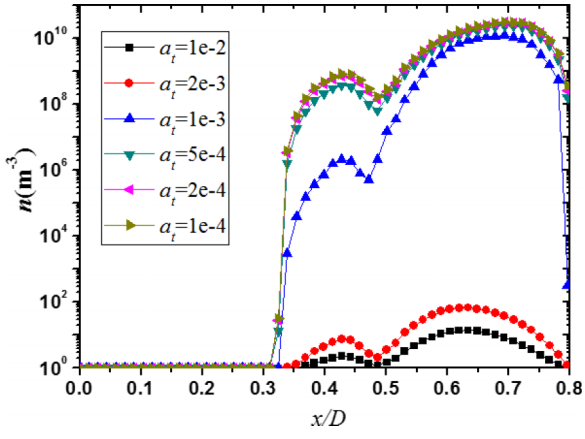

FIG. 20. Bubble number density distribution for different a_t ($b_t = 10^{-6}$ m^2).

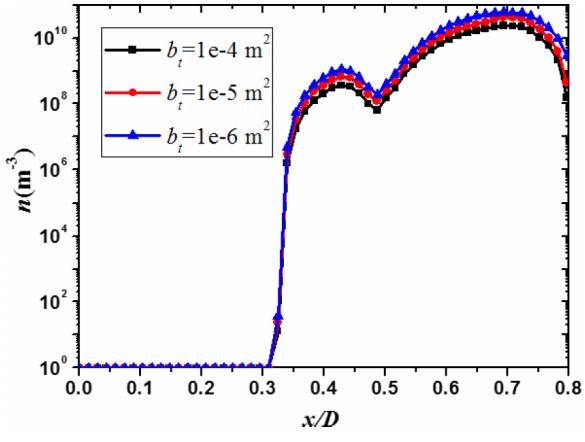

FIG. 21. Bubble number density distribution for different b_t ($a_t = 5\times10^{-4}$).

density rarely changes in the same period of evolution of cavitation when $t' \gg 1$. If $t' \approx 1$, the bubble breakup time is close to the characteristic time of development of the re-entrant jet. Thus, bubble breakup continuously proceeds after sweeping over of the re-entrant jet.

According to the experimental observation, in which cloud cavitation is formed as soon as the re-entrant jet sweeps over, $t' \ll 1$ is presumably obtained. The characteristic time of the

development of the re-entrant jet is $T_c \sim 10^{-3}$, with regard to the cases in the present work. Thus, the bubble breakup time should satisfy $\tau(r) \ll 10^{-3}$.

For all the testing cases in the present paper, the value of turbulent kinetic energy inside the cavitation area is of the order O(1). Thus, k is set as 1 m^2/s^2. According to Eq. (12), the parameter b_t in the model determines bubble size corresponding to the minimum bubble breakup time, which is $r = \sqrt{b_t}$ (Figure 18). The parameter a_t is a relaxation factor that determines the average value of bubble breakup time (Figure 19).

Figures 20 and 21 present the distributions of bubble number density for different a_t and multi-phase values, respectively. The average bubble breakup time significantly affects the distribution of bubble number density, whereas the effect of b_t is limited.

We assume $a_t \leq 10^{-3}$ and $b_t = 10^{-6}$ m^2 to satisfy the requirement for $\tau(r)$. As a result, $a_t = 5 \times 10^{-4}$ and $b_t = 10^{-6}$ m^2 were used for cavitation simulations in the current work.

NOMENCLATURE

A	radius of the bubble cluster,
a_{cr}	critical bubble size,
a_t, b_t	constants for bubble breakup time,
C_e, C_c	constants for phase change rates,
C_f	drag coefficient of a spherical bubble,
C_p	pressure coefficient,
C_μ	constant for turbulence length scale,
D	diameter of projectile,
f_v	mass fraction of vapor,
$f(t,r)$	probability density function of bubble size at time t,
k	turbulent kinetic energy,
L	turbulence length scale,
n	bubble number density,
R, r, r_1	radius of bubble,
$\bar{r}$	average bubble size,
Re	vapor generation rate,
Rc	condensation rate,
Re	Reynolds number,
S_n	source term for transport equation of bubble number density,
p	pressure,
p_B	pressure inside bubble,
p_∞	pressure at infinity,
p_v	phase change threshold pressure,
p_{sat}	saturation pressure of vapor,
$P(t,r)$	turbulent kinetic energy distribution,
$\vec{u}_m$	equivalent velocity of mixture phase,

Greek

α_g	volume fraction of non-condensable gas,
α, α_v	volume fractions of vapor,
β	volume fraction of non-condensable gas,
ε	turbulent dissipation rate,
Γ_m	diffusion coefficient,
μ_m	equivalent viscosity of mixture phase,
μ_v	viscosity of vapor,
μ_g	viscosity of gas,
μ_l	viscosity of liquid,
$\theta(x)$	step function,
ρ_m	density of mixture phase,

ρ_l	density of liquid,
ρ_a, ρ_g	density of gas,
σ	surface tension,
σ_f, σ_p	standard deviation of Gaussian distribution,
$\sum$	cavitation number,
$\tau(r)$	bubble breakup time of a bubble of radius r,
$\omega(r, R)$	bubble breakup function.

[1] G. Bark, M. Grekula, R. Bensow *et al.*, "On some physics to consider in numerical simulation of erosive cavitation," in International Symposium on Cavitation, Singapore, 2011.
[2] K. H. Kim, G. Chahine, J. P. Franc, and A. Karimi, "Advanced experimental and numerical techniques for cavitation erosion prediction," Fluid Mech. Its Appl. **106**, 3–20 (2014).
[3] C. E. Brennen, *Cavitation and Bubble Dynamics* (Oxford University Press, 1995).
[4] V. H. Arakeri and A. J. Acosta, "Viscous effects in the inception of cavitation on axisymmetric bodies," J. Fluids Eng. **95**(4), 519–527 (1973).
[5] V. H. Arakeri, "Viscous effects on the position of cavitation separation from smooth bodies," J. Fluid Mech. **68**(04), 779–799 (1975).
[6] H. Higuchi, R. E. A. Arndt, and M. F. Rogers, "Characteristics of tip vortex cavitation noise," J. Fluids Eng. **111**(4), 495–501 (1989).
[7] J. S. Carlton, *Marine Propellers and Propulsion* (Butterworth-Heinemann, 2012), ISBN: 978-0-7506-8150-6.
[8] G. Wang, I. Senocak, S. Wei *et al.*, "Dynamics of attached turbulent cavitating flows," Prog. Aerosp. Sci. **37**(6), 551–581 (2001).
[9] R. E. A. Arndt, A. Keller, and M. Kjeldsen, "Unsteady operation due to cavitation," in Proceedings of 20th IAHR Symposium on Hydraulic Machinery and Systems, Charlotte, 2000.
[10] S. Gopalan and J. Katz, "Flow structure and modeling issues in the closure region of attached cavitation," Phys. Fluids **12**(4), 895–911 (2000).
[11] T. M. Pham, F. Larrarte, and D. H. Fruman, "Investigation of unsteady sheet cavitation and cloud cavitation mechanisms," J. Fluids Eng. **121**(2), 289–295 (1999).
[12] D. F. de Lange and G. J. de Bruin, "Sheet cavitation and cloud cavitation, re-entrant jet and three-dimensionality," Appl. Sci. Res. **58**, 91–114 (1998).
[13] O. Coutier-Delgosha, B. Stutz, A. Vabre, and S. Legoupil, "Analysis of cavitating flow structure by experimental and numerical investigations," J. Fluid Mech. **578**, 171–222 (2007).
[14] A. Kubota and H. Kato, "Unsteady structure measurement of cloud cavitation on a foil section," J. Fluids Eng. **111**(3), 204–210 (1989).
[15] C. L. Merkle, J. Feng, and P. E. O. Buelow, "Computational modeling of the dynamics of sheet cavitation," in Proceedings of 3rd International Symposium on Cavitation, Grenoble, France, 2001.
[16] R. F. Kunz, D. A. Boger, D. R. Stinebring, T. S. Chyczewski, J. W. Lindau, H. J. Gibeling, S. Venkateswaran, and T. R. Govindan, "A preconditioned Navier-Stokes method for two-phase flows with application to cavitation prediction," Comput. Fluids **29**(8), 849–875 (2000).
[17] A. K. Singhal, M. M. Athavale, H. Li, and Y. Jiang, "Mathematical basis and validation of the full cavitation model," J. Fluids Eng. **124**(3), 617–624 (2002).
[18] F. Örley, V. Pasquariello, S. Hickel, and N. A. Adams, "Cut-element based immersed boundary method for moving geometries in compressible liquid flows with cavitation," J. Comput. Phys. **283**, 1–22 (2015).
[19] C. P. Egerer, S. J. Schmidt, S. Hickel, and N. A. Adams, "Efficient implicit LES method for the simulation of turbulent cavitating flows," J. Comput. Phys. **316**, 453–469 (2016).
[20] M. Gavaises, F. Villa, P. Koukouvinis, M. Marengo, and J. P. Franc, "Visualisation and les simulation of cavitation cloud formation and collapse in an axisymmetric geometry," Int. J. Multiphase Flow **68**, 14–26 (2015).
[21] J. C. Lasheras, C. Eastwood, C. Martínez-Bazán, and J. L. Montañés, "A review of statistical model for the break-up of an immiscible fluid immersed into a fully developed turbulent flow," Int. J. Multiphase Flow **28**, 247–278 (2002).
[22] C. Martínez-Bazán, J. L. Montañés, and J. C. Lasheras, "On the breakup of an air bubble injected into a fully developed turbulent flow. Part 1: Breakup frequency," J. Fluid Mech. **401**, 157–182 (1999).
[23] C. Martínez-Bazán, J. L. Montañés, and J. C. Lasheras, "On the breakup of an air bubble injected into a fully developed turbulent flow. Part 2: Size PDF of the resulting daughter bubbles," J. Fluid Mech. **401**, 183–207 (1999).
[24] G. M. Evans, P. M. Machniewski, and A. K. Bin, "Bubble size distribution and void faction in the wake region below a ventilated gas cavity in downward pipe flow," Chem. Eng. Res. Des. **82**(9), 1095–1104 (2004).
[25] B. Stutz and J. L. Reboud, "Two-phase flow structure of sheet cavitation," Phys. Fluids **9**(12), 3678–3686 (1997).
[26] B. Stutz and J. L. Reboud, "Experiments on unsteady cavitation," Exp. Fluids **22**(3), 191–198 (1997).
[27] B. Stutz and J. L. Reboud, "Measurements within unsteady cavitation," Exp. Fluids **29**(6), 545–552 (2000).
[28] S. Dabiri, W. A. Sirignano, and D. D. Joseph, "Interaction between a cavitation bubble and shear flow," J. Fluid Mech. **651**(3), 93–116 (2010).
[29] G. Wang and M. Ostoja-Starzewski, "Large eddy simulation of a sheet/cloud cavitation on a NACA0015 hydrofoil," Appl. Math. Modell. **31**(3), 417–447 (2007).
[30] V. A. Sosinovich, V. A. Tsyganov, B. A. Kolovandin, B. I. Puris, and V. A. Gertsovich, "Model of gas bubble breakup in turbulent liquid flow," J. Eng. Phys. Thermophys. **68**(2), 164–175 (1995).
[31] V. G. Levich, *Physicochemical Hydrodynamics (English translation by Scripta Technica)* (Prentice-Hall, Englewood Cliffs, USA, 1962).

[32] V. A. Sosinovich, V. A. Tsyganov, B. I. Puris, and V. A. Gertsovich, "Model of fractionation and coalescence of gas bubbles in a turbulent liquid flow," J. Eng. Phys. Thermophys. **70**(6), 918–926 (1997).
[33] M. S. Plesset, "The dynamics of cavitation bubbles," J. Appl. Mech. **16**, 277–282 (1949).
[34] Y. P. Wei, Y. W. Wang, X. Fang, C. G. Huang, and Z. P. Duan, "A scaled underwater launch system accomplished by stress wave propagation technique," Chin. Phys. Lett. **28**(2), 024601 (2011).
[35] Z. Zeravcic, D. Lohse, and W. van Saarloos, "Collective oscillations in bubble clouds," J. Fluid Mech. **680**, 114–149 (2011).
[36] G. E. Reisman and C. E. Brennen, "Shock wave measurements in cloud cavitation," in Proceedings of 21st International Symposium on Shock Waves, Paper 1570, 1997.
[37] G. E. Reisman, Y. C. Wang, and C. E. Brennen, "Observations of shock waves in cloud cavitation," J. Fluid Mech. **355**, 255–283 (1998).
[38] Y. Murai, "Frictional drag reduction by bubble injection," Exp. Fluids **55**, 1173 (2014).
[39] Y. C. Wang and C. E. Brennen, "The noise generated by the collapse of a cloud of cavitation bubbles," in *ASME Symposium on Cavitation and Gas-Liquid Flows in Fluid Machinery and Devices, ED 226* (ASME, 1995), pp. 17–29.
[40] Y. C. Wang and C. E. Brennen, "Shock wave and noise in the collapse of a cloud of cavitation bubbles," in *Proceedings of 20th International Symposium on Shock Waves*, *Pasadena* (World Scientific, 1995), pp. 1213–1218.
[41] L. Zhang, Z. Wen, and X. Shao, "Investigation of bubble-bubble interaction effect during the collapse of multi-bubble system," Chin. J. Theor. Appl. Mech. **45**(6), 861–867 (2013).
[42] Y. C. Wang, "Distribution on the dynamics of a spherical cloud of cavitation bubbles," J. Fluids Eng. **121**, 881–886 (1999).